

# On the origin of the high velocity SiO maser emission from late-type stars

F. Herpin<sup>1</sup>, A. Baudry<sup>1</sup>, J. Alcolea<sup>2</sup>, J. Cernicharo<sup>3</sup>

<sup>1</sup> Observatoire de Bordeaux, BP 89, F-33270 Floirac, France

<sup>2</sup> Observatorio Astronómico Nacional, Apartado 1143, E-28800 Alcalá de Henares, Spain

<sup>3</sup> CSIC, IEM, Depto. Física Molecular, Serrano123, E-28006 Madrid, Spain

Received 28 October 1997; accepted 3 March 1998

**Abstract.** We have undertaken toward 30 Mira or semi-regular variables and one OH/IR object highly sensitive observations of the  $v = 1, J = 2 \rightarrow 1$  and  $3 \rightarrow 2$  transitions of SiO simultaneously with observations of the  $J = 1 \rightarrow 0$  transition of CO during three observing sessions in the period 1995 to 1996. As in our previous observations of 1994, we observe that for several stars the SiO profiles exhibit unusually broad wings which sometimes exceed the terminal velocity of the expanding circumstellar envelope traced by the thermal CO emission. We have discovered a clear dependence of the SiO wing emission on the optical phase. These wings are probably due to peculiar gas motions and varying physical conditions in relation with the stellar pulsation. However, we cannot exclude other mechanisms contributing to the observed wings. In particular, SiO turbulent motions for the semi-regular variables or the asymmetric mass loss mechanism may play a role. We conclude that the SiO wing emission is due to masing processes and that this emission very likely arises from the inner part of the circumstellar envelope.

**Key words:** Stars: late-type, circumstellar matter; Masers: SiO; Line: SiO, CO profiles, formation

stars, we discovered unexpectedly broad wing SiO emission (Cernicharo et al. 1997, hereafter referred as CABG). We found that the  $v = 1, J = 2 \rightarrow 1$  SiO emission reaches and sometimes exceeds the maximum velocity traced by the quasi-thermal emission of the CO molecule. Several mechanisms may be invoked to explain such wings: turbulent motions, rotation of dense SiO clumps, high velocity shocks produced during the pulsation of the star, or high velocity bipolar ejection of gas from the star. These mechanisms were discussed by CABG, but no firm conclusions were reached, although it was recognized that the pulsation of the star and asymmetric mass loss could play an important role. Obviously interferometric observations and a monitoring of the SiO wing emission are needed to shed light on the location and the physical origin of the high velocity SiO emission.

The main purpose of this paper is to present and analyze new data gathered at different epochs on the SiO velocity wings in order to study the physical mechanisms responsible for this phenomenon, and, at the same time, to obtain deeper insight into the complex kinematics of the circumstellar shells around late-type stars. The latter question is clearly important since it is related to other crucial problems such as the expansion of the CE and the mass loss phenomenon, or the processes leading to the formation of dust. We have considered a rather small but homogeneous sample of stars as it includes Miras and a few semi-regulars for which all stellar characteristics (mass loss, temperature, spatial distribution . . .) are uniformly represented. We have monitored the SiO maser line profiles in order to investigate the relation of broad (weak) emission in wings with the stellar light phase. In particular, we wish to test whether the shocks driven by the stellar pulsation could play a dominant role in the occurrence of SiO high velocity features. In Sects. 2 and 3 we give details of our observations and present our main results. In Sect. 4 we discuss the different hypotheses which could explain the SiO line wings and their location.

## 1. Introduction

The SiO molecule exhibits widespread maser emission from O-rich circumstellar envelopes (CEs) around Long Period Variables (LPVs). The variety of rotational transitions emitted from several vibrational levels and the strength of the emission make these lines very useful for a study of the innermost layers of CEs. Recently, during sensitive SiO observations of several O-rich late-type

---

Send offprint requests to: F. Herpin, herpin@observ.u-bordeaux.fr

arXiv:astro-ph/9803032v1 4 Mar 1998

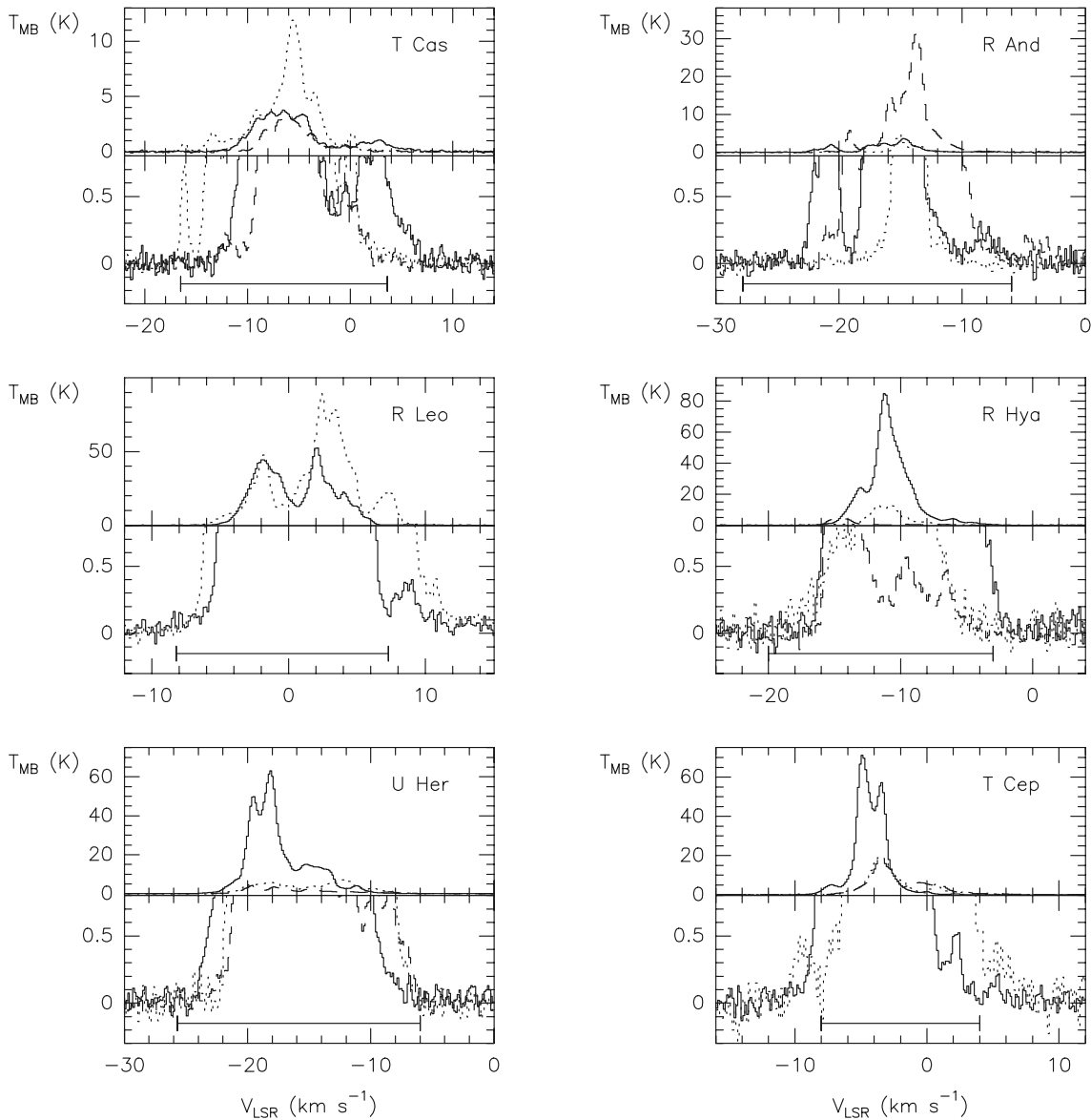


**Fig. 1.** Examples of SiO  $v = 1, J = 2 \rightarrow 1$  spectra for *Mira variables* taken with  $0.136 \text{ km s}^{-1}$  spectral resolution in June 1995 (continuous line), April 1996 (dashed line) and October 1996 (dotted line). For each star the top panel shows the full main beam brightness temperature scale and the bottom panel corresponds to an enlargement of the same data, with the CO line emission width ( $\Delta V(\text{CO})$  above the  $2\sigma$  level) represented by a horizontal segment. For R Leo, no data are available for April 1996. To transform the intensities into Jy one must multiply by  $4.4 \text{ Jy/K}$ .

## 2. Observations

Our observations were carried out with the IRAM 30-m telescope in June 1995 and in April and October 1996. They were combined with our earlier observations of January 1994 first presented by CABG. The sample of selected Mira and semi-regular variable stars was identical for all epochs, apart from a few exceptions. The supergiant VY CMa was not observed in 1995 and 1996. In

June 1995 and later, we added the Mira variable  $\chi$  Cyg to our sample. In this work, we have observed just one OH/IR object, OH127.8 – 0.0, at one epoch only, June 1995. The sample of sources discussed here is listed in the first column of Table 1. Two SIS receivers were used simultaneously at 86.243 and 230.538 GHz to observe the SiO  $v = 1, J = 2 \rightarrow 1$  and the CO  $J = 2 \rightarrow 1$  lines. In 1995 and 1996 we added a third receiver to observe the SiO  $v = 1, J = 3 \rightarrow 2$  line at 129.363 GHz. To properly detect

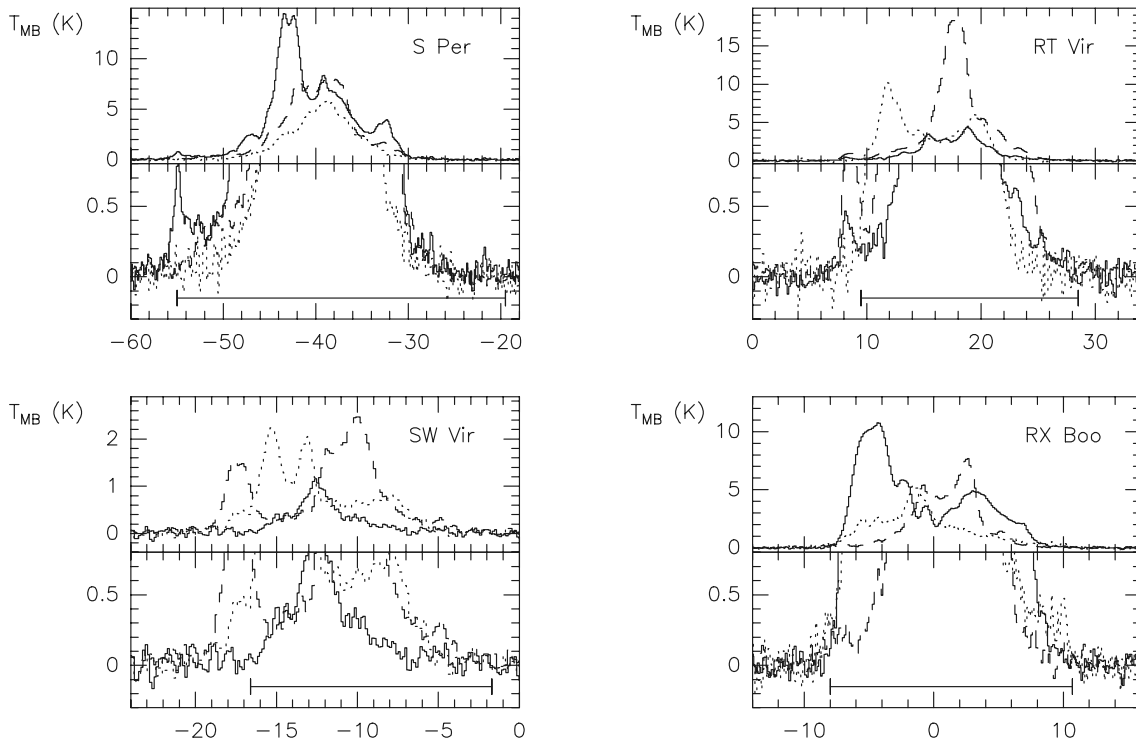


**Fig. 2.** Examples of SiO  $v = 1, J = 2 \rightarrow 1$  spectra for *Semi-Regular variables* taken with  $0.136 \text{ km s}^{-1}$  spectral resolution in June 1995 (continuous line), April 1996 (dashed line) and October 1996 (dotted line). For each star the top panel shows the full main beam brightness temperature scale and the bottom panel corresponds to an enlargement of the same data, with the CO line emission width ( $\Delta V(\text{CO})$  above the  $2\sigma$  level) represented by a horizontal segment. To transform the intensities into Jy one must multiply by  $4.4 \text{ Jy/K}$ .

and analyze weak SiO line wing signals we adjusted the side-band noise level of the receiver phase-lock loops below  $-35 \text{ dB}$ . The 3, 2 and 1 mm receivers were SSB tuned and the attenuations of the image band were of order 35 and 7 dB for the 3 and 2 mm SiO lines, and 30 dB for the CO line. The best observing period was that of January 1994 (CABG) with low ambient temperature (nearly  $-10^\circ \text{ C}$ ) and almost no humidity. For the three other epochs the observations were made with clear sky but with relative humidity in the range 30 – 70%. Depending on the source elevation and on the epoch, the SSB system temperatures were in the range 140 – 400, 270 – 600 and 180 – 1000 K for the 3, 2 and 1 mm receivers, respectively. Line calibration was deduced from regular observations of a hot and cold load and from measurements of the sky emissivity. In this work the line intensities are calibrated in terms of the main beam brightness temperature. For the observations of 1995 and 1996 we adopted 0.75 and 0.58 for the telescope main beam efficiencies at the frequencies of the SiO  $v = 1, J = 2 \rightarrow 1$  and  $J = 3 \rightarrow 2$  lines, respectively. In 1994 we used 0.60 for the 3 mm observations (CABG). These intensities (in K) can be transformed into flux densities (in Jy) by multiplying by 4.4 at 3 and 2 mm. In gen-

eral, the pointing corrections were determined by cross scanning the 3 mm maser line itself, using several filter channels as a continuum detector. The absolute pointing of the 3 mm receiver and the alignment between all receivers lay in the range  $2 - 4''$ . The focus adjustment was regularly monitored. For spectral analysis we used analog filters with both low (1 MHz) and high (100 kHz) resolution and the 2048-channel autocorrelator. The resolution thus achieved was  $3.5, 0.35, 0.136$  and  $0.07 \text{ km s}^{-1}$  in SiO ( $J = 2 - 1$ ),  $0.18$  and  $2.3 \text{ km s}^{-1}$  in SiO ( $J = 3 - 2$ ) and  $1.3, 0.4, 0.1$  and  $0.05 \text{ km s}^{-1}$  in CO ( $J = 2 - 1$ ). We checked that by smoothing the autocorrelator channels to a resolution similar to that given by the filterbank channels the linewidths were identical. Because we searched for line wing emissions as weak as a few tens of mK flat spectral baselines are essential. All observations were thus made with the wobbling secondary mirror system. Figures 1 and 2 shows examples of SiO  $v = 1, J = 2 \rightarrow 1$  spectra obtained in 1995 and 1996. Note that the quality of the spectral baselines facilitates the comparison of the CO and SiO line wings.

**Table 1.** Selected stars and observed line parameters for the SiO  $v = 1, J = 2 \rightarrow 1$  and  $v = 1, J = 3 \rightarrow 2$  emissions observed in June 1995. Stars are arranged in ascending right ascension order. To transform the peak line intensities into Jy one must multiply the observed  $J = 2 - 1$  and  $J = 3 - 2$  values of  $T_{MB}$  by 4.4 Jy/K.

Stars	Stellar Class	SiO $v=1$ $J=2-1$ (June 1995)					SiO $v=1$ $J=3-2$ (June 1995)				
		$\sigma$ mK	$T_{MB}$ K	$V_{LSR}$ kms $^{-1}$	$\Delta V(2\sigma)$ kms $^{-1}$	$\int T_{MB}dV$ Kkms $^{-1}$	$\sigma$ mK	$T_{MB}$ K	$V_{LSR}$ kms $^{-1}$	$\Delta V(2\sigma)$ kms $^{-1}$	$\int T_{MB}dV$ Kkms $^{-1}$
Y Cas	Mira	34	7.3	-19.1	15.3	26	51	3.9	-18.8	10.4	12
T Cas	Mira	33	3.7	-6.4	19.8	27	53	1.3	2.7	14.3	5
R And	Mira	32	3.4	-14.8	18.5	15	49	2.1	-17.2	14.9	6
IRC+10011	Mira	38	11.6	6.7	9.7	30	57	5.1	7.9	8.1	11
<i>o</i> Ceti	Mira	25	82.9	43.3	14.2	420	41	26.1	48.1	9.8	59
S Per	SRc	39	14.5	-43.2	32.0	107	56	4.3	-32.0	25.8	36
NML Tau	Mira	59	87.9	35.7	13.2	343	114	46.3	36.2	9.3	148
TX Cam	Mira	85	38.3	10.2	12.4	118	51	15.1	11.7	10.7	38
U Ori	Mira	38	2.3	-36.8	13	13	72	4.1	-44.6	9.8	6
V Cam	Mira	44	6.4	6.5	18.3	22	82	2.4	7.2	10.1	6
GX Mon	Mira	41	9.7	-10.0	13.0	36	73	5.0	-9.1	12.3	16
S CMi	Mira	31	2.3	50.1	11.5	8	92	0.4	54.4	4.5	1
W Cnc	Mira	35	1.3	34.8	10.8	6	87	0.6	35.7	2.8	1
R LMi	Mira	30	10.7	-3.8	15.8	48	51	2.4	1.1	10.9	11
R Leo	Mira	52	50.2	2.0	15.8	260	52	19.4	-0.8	13.7	69
R Crt	SRb	36	5.1	8.7	25.1	39	65	1.0	6.1	16.0	6
RT Vir	SRb	30	4.3	18.9	20.0	25	56	0.9	15.8	10.9	4
SW Vir	SRb	35	1.1	-12.4	11.2	4					
R Hya	Mira	46	83.6	-11.2	15.3	237	111	27.1	-10.7	14.3	90
W Hya	SRa	42	64.4	41.7	16.7	382	99	72.9	42.3	18.2	229
RX Boo	SRb	35	10.8	-4.4	18.2	72	55	0.5	1.2	7.9	1
S CrB	Mira	54	7.0	0.3	11.5	16	65	0.2	-1.0	5.1	1
RU Her	Mira	33	3.9	-10.6	15.1	21	66	2.3	-17.8	14.0	8
U Her	Mira	45	61.3	-18.1	16.4	221	50	8.1	-18.5	14.3	58
VX Sgr	SRc	47	30.3	7.2	35.9	263	74	15	0.0	33.1	139
R Aql	Mira	33	2.9	50.3	16.1	18	62	0.5	44.4	8.1	2
$\chi$ Cyg	Mira	55	29.0	11.1	16.4	93	53	19.3	11.8	18.2	73
T Cep	Mira	36	67.2	-5.1	16.1	167	55	6.4	-3.3	12.1	17
$\mu$ Cep	SRc	39	8.5	24.1	18.0	56	52	15.6	25.0	18.2	62
R Cas	Mira	35	40.3	25.4	15.0	126	54	4.8	30.0	14.9	22
OH127.8-0.0	OH/IR	31	0.4	-56.5	8.3	1	15	0.1	-58.3	10.2	0.6

### 3. Results

#### 3.1. SiO $v = 1, J = 2 \rightarrow 1$ emission

In Table 1 we present the SiO  $v = 1, J = 2 \rightarrow 1$  line parameters of sources observed in June 1995 (including OH127.8 - 0.0 at the bottom of Table 1). The line parameters for April and October 1996 are given in Herpin (Ph.D. Thesis 1998). The SiO and CO line parameters of 1994 are given in Table 1 of CABG. In column 2 of Table 2 of the present work we also list the line width above the  $2\sigma$  noise level of the CO observations made in 1994 because they are used as our CO reference data. Although the atmosphere was less transparent at the CO(2-1) line in 1995 and 1996 than in 1994 we verified that the CO central velocity and linewidth remained constant with the epoch of the observations within a few %. The SiO main beam brightness temperature  $T_{MB}$  and velocity  $V_{LSR}$  given in Table 1 correspond to the strongest emission feature in the spectra. The SiO full linewidth above the  $2\sigma$  spectral noise level  $\Delta V$  is also given in Table 1 for June 1995. As in CABG, our new observations show that several stars exhibit pronounced blue or red wings. This is a firm result because it is confirmed by the different backends and spectral resolutions available on the 30-m. These high velocity wings (e.g. Figs. 1 and 2) are weak compared to

the bulk of the SiO  $v = 1, J = 2 \rightarrow 1$  emission whose central velocity is close to the CO central velocity; the latter gives the systemic velocity of the underlying star. We have no direct proof at the moment that the SiO line wing emission is masing as are the main velocity features. We note that  $v = 1$  thermal lines would be very difficult to detect at these high velocities where no thermal SiO emission is observed in the ground vibrational state (Cernicharo et al.1994, Bujarrabal et al.1989). Furthermore, in the case of R Leo (CABG) and some other stars, the linewidths are polarized. This indicates maser amplification, a fact strengthened by the line variability of the line wing emission discussed in Sect. 4.

To compare the velocity extent of the  $v = 1, J = 2 \rightarrow 1$  emission of SiO with the CO(2-1) total velocity extent we define the ratio  $R_{21} = \Delta V(\text{SiO}(2-1))/\Delta V(\text{CO}(2-1))$  where  $\Delta V$  is the full width of the emission above the  $2\sigma$  noise level at the epoch of the observations;  $\Delta V(\text{CO}(2-1))$  always refers to our 1994 observations. The values of  $R$  are given with additional comments in Table 2 for the 1994, 1995 and 1996 results. Because the CO profile delineates regions of the circumstellar envelope where the gas reaches its maximum velocity whereas the SiO velocities trace layers close to the photosphere, the ratio  $R_{21}$  gives direct information on the kinematics of the inner circum-

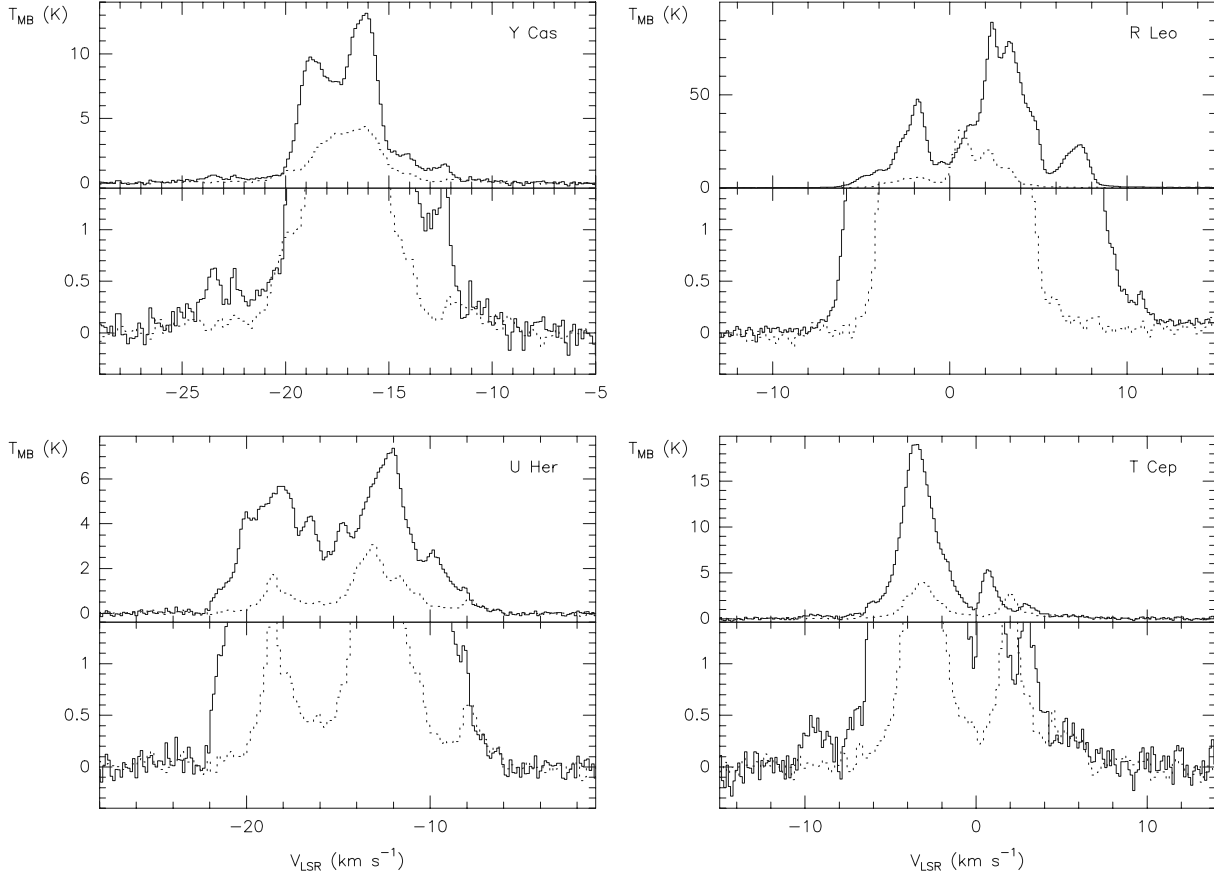


**Fig. 3.** SiO  $v = 1, J = 3 \rightarrow 2$  spectra (dashed line) observed toward Y Cas, U Her, R Leo and T Cep superposed on the  $J = 2 \rightarrow 1$  spectra (continuous line) in the same stars. For each star the top panel shows the full main beam brightness temperature and the bottom panel corresponds to an enlargement of the same data. The epoch of the observations was October 1996 and the spectral resolution was  $0.136 \text{ km s}^{-1}$  for the  $J = 2 \rightarrow 1$  line and  $0.181 \text{ km s}^{-1}$  for the  $J = 3 \rightarrow 2$  line. To transform the intensities into Jy one must multiply by  $4.4 \text{ Jy/K}$  for both transitions.

stellar layers. As indicated earlier, for a given star and at each epoch, the quantity  $\Delta V(\text{CO}(2-1))$  does not vary with time in contrast with  $\Delta V(\text{SiO})$ .  $\Delta V(\text{CO}(2-1))$  is unambiguously determined although in a few cases there may be contamination by interstellar CO (see CABG for discussion); these cases are marked with an asterisk in Table 2. Several stars have high  $R_{21}$  values and some of them exhibit prominent red or blue SiO wings, i.e. the SiO velocity exceeds the thermal CO velocity on the red or blue spectral end; these cases are noted R or B in Table 2. More than one half of our sample shows a B or R SiO wing. The presence of red wings in the SiO spectra indicates that there is gas emission at high velocities not observed in the thermal CO gas. Interpretation of the SiO blue wings is less straightforward because of possible self-absorption in the blue wing of the CO line profile (Huggins & Healy 1986). Therefore, the detection of SiO blue wings may not necessarily mean that the CE terminal velocity

is exceeded. If we restrict our sample of stars to Miras only, the average value of  $R_{21}$  is  $\overline{R}_{21} = 0.70, 0.75, 0.85$  and  $0.86$  for the epochs 1994, 1995 and April and October 1996. The same quantities are systematically higher for the semi-regular variables:  $\overline{R}_{21} = 1.04, 0.85, 1.04$  and  $0.94$ . Nearly half of the observed stars have  $R_{21} \geq \overline{R}_{21}$  and 15 to 30 % have  $R_{21} \geq 1$ . On the other hand, several stars, IRC+10011, NML Tau, TX Cam, V Cam, GX Mon,  $\chi$  Cyg and R Cas have small  $R_{21}$  values. This is perhaps due to observations made roughly at the same stellar phase for NML Tau, TX Cam, V Cam and GX Mon. However, some stars have low or moderate and nearly constant  $R_{21}$  values at all phases ( $\chi$  Cyg, R Cas and IRC+10011). We note that  $\chi$  Cyg is an S-star and therefore presents many peculiarities in the pumping of its masers (see Bujarrabal et al. 1996). Some others have quite high  $R_{21}$  values (e.g. T Cep and RU Her with  $R_{21} = 2.21$  and  $2.24$  in April and October 1996, respectively).

**Table 2.** Total linewidth ratios at the four epochs of the observations. The epochs a,b,c,d correspond to Jan. 1994, June 1995, April and October 1996, respectively and ND means no data available.  $\Delta V(CO)$  above the  $2\sigma$  noise level is given in column 2 of this Table and refer to the 1994 observations (Cernicharo et al.1997). The mass loss  $\dot{M}$  is taken from Loup et al.(1993). Stars are arranged in ascending right ascension order. Comments : (\*) CO line contaminated by galactic emission ; (R) or (B) means that the SiO red or blue wing reaches or surpasses respectively the most positive or negative CO velocity.

Stars	$\Delta V(CO)_{2\sigma}$ kms <sup>-1</sup>	$\dot{M}$ M <sub>⊙</sub> /year	Stellar phase				$R_{21} = \frac{\Delta V(SiO(2-1))}{\Delta V(CO(2-1))}$				$R_{32} = \frac{\Delta V(SiO(3-2))}{\Delta V(CO(2-1))}$		
			a	b	c	d	a	b	c	d	b	c	d
Y Cas	23.6	ND	0.86	0.11	0.80	0.24	0.63 R	0.65	0.68	0.72	0.44	0.20	0.74 R
T Cas	20.0	5.1 10 <sup>-7</sup>	0.83	0.004	0.68	0.10	0.56	0.99 R	0.69	1.15 RB	0.71 R		1.00 B
R And	21.8	9.6 10 <sup>-7</sup>	0.15	0.38	0.13	0.58	0.93 R	0.85	0.58	0.42	0.68		
IRC+10011	39.3	8.5 10 <sup>-6</sup>	0.65	0.44	0.90	0.19	0.30	0.25	0.36	0.27	0.21		0.30
OH127.8-0.0	22.7	1.5 10 <sup>-6</sup>	ND	ND			0.21 *	0.36 *			0.45		
o Ceti	18.7	5.0 10 <sup>-7</sup>	0.52	0.94		0.67	0.44	0.85		0.80	0.52		0.64
S Per	35.9	ND	0.40	0.08	0.48	0.71	0.94 *B	0.89 *B	0.88 *B	0.69 *B	0.72 *		0.56
NML Tau	40.8	4.4 10 <sup>-6</sup>	0.13	0.24		0.29	0.41	0.32		0.33	0.23		0.39
TX Cam	40.8	2.5 10 <sup>-6</sup>	0.33	0.16		0.34	0.32	0.30		0.46	0.26		0.41
U Ori	16.9	ND	0.22	0.66		0.97	1.10 RB	0.74 B		1.04 *B	0.58		0.69 *
V Cam	31.1	1.6 10 <sup>-6</sup>	0.43	0.46		0.39	0.50	0.59		0.45	0.32		0.34
GX Mon	39.2	5.4 10 <sup>-6</sup>	0.40	0.39		0.28	0.28	0.33		0.45	0.32		0.48
S CMi	7.2	ND	0.69	0.14		0.53	1.33 R	1.60 RB		1.68 R	0.62 R		
W Cnc	15.7	ND	0.94	0.24		0.50	0.92 R	0.69		0.78 R	0.18		
R LMi	19.5	2.8 10 <sup>-7</sup>	0.34	0.70		0.16	0.70 R	0.81 R		0.85 R	0.56		
R Leo	15.7	1.0 10 <sup>-7</sup>	0.63	0.29		0.85	1.00 RB	1.00 R		1.20 R	0.87 R		0.91 R
R Crt	23.5	7.5 10 <sup>-7</sup>	ND	ND		ND	0.82 B	1.07 B		0.92	0.68		
RT Vir	18.8	7.4 10 <sup>-7</sup>	0.95	0.58	0.56	0.77	1.22 B	1.06 B	1.14 B	0.87	0.58		0.60
SW Vir	14.9	5.7 10 <sup>-7</sup>	0.69	0.05	0.98	0.27	0.55	0.75	1.22 B	1.13 B			
R Hya	15.9	1.4 10 <sup>-7</sup>	0.92	0.30	0.00	0.57	0.53	0.96 R	0.95 R	0.85	0.90 R		0.40
W Hya	17.2	8.1 10 <sup>-8</sup>	0.68	0.01	0.92	0.34	1.30 RB	0.97 B	1.00 RB	0.97 B	1.06 R		
RX Boo	19.5	8.1 10 <sup>-7</sup>	0.81	0.21	0.99	0.67	0.65	1.06 B	1.05 RB	1.03 *RB	0.41	0.46	0.30 *
S Crb	15.0	5.8 10 <sup>-7</sup>	0.26	0.74	0.51	0.03	0.95 R	0.77	1.00 B	1.17 B	0.34		0.69
RU Her	16.4	ND	0.10	0.17	0.81	0.19	0.85 R	0.92 B	0.93 B	2.24 R	0.85	0.34	0.67
U Her	19.9	2.6 10 <sup>-7</sup>	0.66	0.03	0.77	0.23	0.74	0.82	0.89 R	0.92	0.72	0.61	0.97 R
R Aql	18.8	3.6 10 <sup>-7</sup>	0.004	0.02	0.03	0.69	0.62	0.85 B	0.79 R	0.57 *	0.43		0.38 *
χ Cyg	24.8	5.6 10 <sup>-7</sup>	0.70	0.99	0.75	0.21	0.50	0.66	0.53	0.60	0.73		0.52
T Cep	11.8	1.4 10 <sup>-7</sup>	0.04	0.35	0.13	0.61	1.07 RB	1.36 RB	2.21 RB	1.49 RB	1.02 B		1.19 R
μ Cep	35.9	ND	0.81	0.43		0.65	1.83 *RB	0.50 *		0.84 *B	0.51 *		0.56 *
R Cas	28.8	1.1 10 <sup>-6</sup>	0.35	0.60	0.28	0.71	0.66	0.52	0.59	0.38 *	0.52	0.50	0.23 *

### 3.2. SiO $v = 1, J = 3 \rightarrow 2$ emission

The central velocity of the  $v = 1, J = 3 \rightarrow 2$  emission is often quite different from that of the  $J = 2 \rightarrow 1$  emission as one would expect in gas layers with different excitation conditions. With a few exceptions, the line intensities and full linewidths above the  $2\sigma$  noise level for the  $J = 3 \rightarrow 2$  line are systematically smaller than for the  $J = 2 \rightarrow 1$  line. As an example, in June 1995 we have obtained for the Miras R Leo and U Her,  $T_{MB} = 19.4$  and  $8.1$  K,  $\Delta V = 13.7$  and  $14.3$  kms<sup>-1</sup> in the  $J = 3 \rightarrow 2$  line while we have measured  $T_{MB} = 50.2$  and  $61.3$  K,  $\Delta V = 15.8$  and  $16.4$  kms<sup>-1</sup> in the  $J = 2 \rightarrow 1$  line. Examples of spectra are given in Fig. 3. As for the  $J = 2 \rightarrow 1$  line we define the ratio  $R_{32} = \Delta V(SiO(3-2))/\Delta V(CO(2-1))$ , and we give the individual values of this ratio in the last three columns of Table 3. If we restrict our sample of stars to Miras only, the average value of  $R_{32}$  is  $\bar{R}_{32} = 0.57, 0.41$  and  $0.61$  for the epochs 1995, and April and October 1996. In contrast with  $\bar{R}_{21}$ , the values of  $\bar{R}_{32}$  are not systematically higher for the semi-regular variables:  $\bar{R}_{32} = 0.55, 0.68$  and  $0.52$  for the epochs 1995, and April and October 1996. All values of  $R_{32}$  and  $\bar{R}_{32}$  are lower than the corresponding values derived for the  $J = 2 \rightarrow 1$  line; this reflects the fact

that  $\Delta V(SiO(3-2)) < \Delta V(SiO(2-1))$ . Nevertheless, in June 1995 and October 1996 where 20 to 30 stars were observed at 2 mm, few of them have a value of  $R_{32}$  larger than, or of order 1. The case of T Cep is interesting as the large  $R_{21}$  value observed at 3 mm is also observed at 2 mm (Fig. 3 and Table 2). About 20% of the observed stars show a blue or red SiO wing with a majority of stars exhibiting a red wing (Table 2).

### 3.3. Variability of the ratio $R = \Delta v(SiO)/\Delta v(CO)$

In Table 2 we compare the values of  $R_{21}$  derived for  $\Delta V(SiO(2-1))$  at the four epochs of the observations and we derive the associated stellar phase from the most recent stellar light parameters given by the AFOEV<sup>1</sup>. The stellar period was rather well sampled in general although additional observations would be deserved. Our data show that there is a dependence of  $R_{21}$  with the optical phase for each star. This dependence is clearly not similar for all stars in our sample. Despite the fact that we only have 3 or 4 distinct epochs and that the stellar periods are unequally sampled we have searched for periodicity in our

<sup>1</sup> AFOEV=Association Francaise des Observateurs d'Etoiles Variables

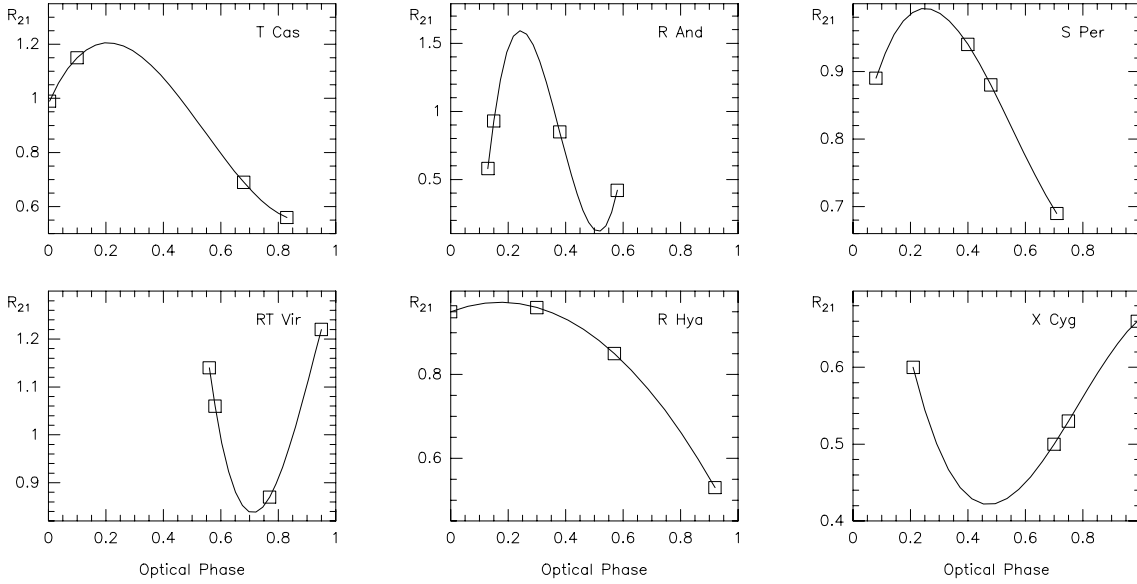


**Fig. 4.** Examples of variations of  $R_{21} = \Delta V(\text{SiO}(2-1))/\Delta V(\text{CO}(2-1))$  with the stellar phase for the semi-regular variables S Per and RT Vir, and the Miras R And, R Hya,  $\chi$  Cyg and T Cas. The linewidths are defined at the  $2\sigma$  noise level.

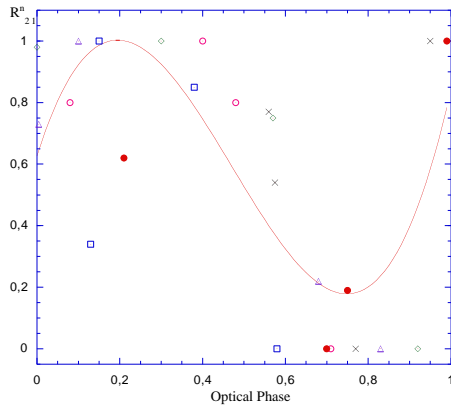


**Fig. 5.** Plot of the normalized ratio  $R_{21}^n = \frac{\Delta V(\text{SiO}(2-1))}{\Delta V(\text{CO}(2-1))}$  versus the stellar phase for the stars plotted in Fig.4. Each type of plot marker corresponds to a different star:  $\bullet = \chi$  Cyg,  $\triangle =$  T Cas,  $\square =$  R And,  $\times =$  RT Vir,  $\diamond =$  R Hya,  $\circ =$  S Per. The fit is a third degree polynomial.

data by fitting cubic spline functions. We show six examples in Fig. 4. In several cases  $R_{21}$  reaches a maximum and a minimum around the optical phases 0.1 – 0.3 and 0.6 – 0.8, respectively. This maximum activity seems to occur with the same phase lag as that observed for the bulk of the SiO emission (0.2 – 0.3 in general). The general trend above is not always observed. In R Cas or  $\chi$  Cyg

for example,  $R_{21}$  tends to be maximum around 0.0, and in the case of W Hya (SRA)  $R_{21}$  tends to remain roughly constant with time. As the amplitudes of the variations of  $R_{21}$  are obviously different from one star to the other, and because our sample of stars is rather homogeneous, we have normalized these values by forcing the maximum and minimum  $R_{21}$  values for each star to 1.0 and 0.0, respectively; these normalized values,  $R_{21}^n$ , are plotted versus the optical phase in Fig.5. A global trend is obvious with a slight maximum and minimum of  $R_{21}^n$  between optical phases 0.1-0.3 and 0.6-0.8, respectively, as for the individual plots.

In some stars, R And, TX Cam, R Leo, RU Her and R Aql, we have observed a rapid variation in the amplitude of  $R_{21}$ . These variations occur nearly at the same stellar phase but correspond to observations made in 1994, 1995 and 1996, and thus correspond to different stellar pulsation cycles. This suggests that besides the smooth variation of  $R_{21}$  with the stellar pulsation observed in several stars, the SiO wing emission may differ from one optical cycle to the other. We may thus have the combined effect of a smooth stellar pulsation with another mechanism (of a different time order). This remark also applies to R Leo (Fig. 6) for which several epochs are available although on average  $R_{21}$  tends to be maximum and minimum around optical phases 0.2 and 0.5, respectively. Comparing the behaviours of  $R_{21}$  and of the stellar visual magnitude  $m_v$  with time, we note that the sudden amplitude variations of  $R_{21}$  at a given optical phase (as observed for example in R Aql and R Leo near optical phases 0.0 and 0.7 re-

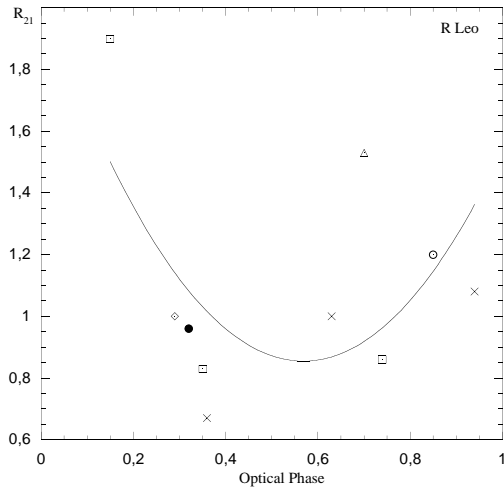


**Fig. 6.** Plot of the ratio  $R_{21} = \Delta V(\text{SiO}(2-1))/\Delta V(\text{CO}(2-1))$  versus the stellar phase for R Leo. The linewidths are defined at the  $2\sigma$  noise level. Each type of plot marker corresponds to a different stellar cycle:  $\bullet$  = April 1991,  $\triangle$  = June 1992,  $\square$  = Nov. 1992 to May 1993,  $\times$  = Nov. 1993 to May 1994,  $\diamond$  = June 1995,  $\circ$  = October 1996.

spectively), occur simultaneously with strong amplitude variations of  $m_v$  from one stellar cycle to the other. In all cases, the sudden increase in  $R_{21}$  corresponds to a luminosity increase which one may relate to IR pumping of these masers.

In Table 2 we also give the ratio  $R_{32}$  and the optical phase at the four epochs of our observations. The general trends observed for  $R_{21}$  are also present in  $R_{32}$ . However, the SiO line wing intensities and extents are smaller in the  $J = 3 \rightarrow 2$  line than in the  $J = 2 \rightarrow 1$  line. RU Her is an extreme case where the conspicuous red wing detected in October 1996 at 3 mm is not present in the 2 mm spectrum.

It is interesting to compare the time variation of the ratio  $R_{21}$  with that of the SiO peak intensity which is associated with the bulk of the emission (characterized by  $T_{MB}$  and the associated central velocity). The SiO main emission is known to vary from one stellar cycle to the other and to reach a maximum somewhat after the optical maximum (e.g. Alcolea 1993, and Martinez et al. 1988). As previously observed by other authors, we also find that  $T_{MB}(\text{SiO}(2-1))$  varies with the optical phase. However, because the stellar cycle is not densely enough sampled it is impossible to conclude that  $R_{21}$  and  $T_{MB}$  vary in phase or not, even if  $R_{21}$  seems to present a maximum

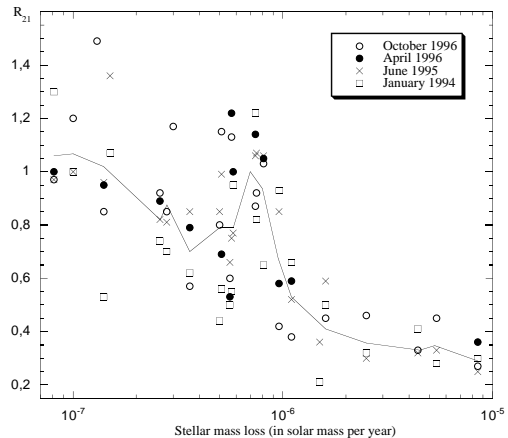


**Fig. 7.** Plot of  $R_{21} = \Delta V(\text{SiO}(2-1))/\Delta V(\text{CO}(2-1))$  versus the stellar mass loss (in  $M_{\odot}/\text{year}$ ) for all observations and all stars. The mass loss is taken from Loup et al.(1993). The solid line connects the averages of all points as determined at individual stellar mass loss values.

and minimum at the same phases as usually observed for the intensity.

## 4. Discussion

In this section we first discuss some of the mechanisms at the origin of the high velocity SiO emission and whether these are consistent with the observed behaviour of the ratio  $R$  with the light cycle. Secondly, we will discuss whether our data bring some evidence or not on the question of the co-location of the SiO wing emission and of the bulk of the SiO emission, and on the influence of the stellar mass loss rate.

### 4.1. Formation of SiO high velocity wings

Various mechanisms, or a combination of these mechanisms, may be invoked to explain the high velocities observed in our SiO spectra: turbulent motions, stellar pulsation, rotation or asymmetric mass loss. These mechanisms were discussed earlier by CABG, mainly they demonstrated the importance of the asymmetric mass loss while the impact of rotation was shown to be minor. In addition, the characteristic profile predicted by rotation (e.g. two- or three-horn profile) is not observed in our SiO spectra. Our new data bring information on the two first mechanisms, namely turbulent motions and stellar pulsation.



#### 4.1.1. Turbulent motions

With the non-local radiative transfer code described by González-Alfonso & Cernicharo (1997), CABG modeled the SiO emission in an expanding envelope with low terminal velocity, high mass loss rate and strong turbulent motions. CABG succeeded in predicting blue wings and weak red wings because of shadowing and amplification of stellar emission. Several stars observed in this work show indeed blue wings without a red counterpart at a given optical phase. This is observed for 7 of the 8 semi-regulars in our sample and for 4 Miras. In the 4 semi-regulars S Per (SRc), R Crt (SRb), RT Vir (SRb) and SW Vir (SRb) we have not detected any red wing at any epoch. Turbulence could thus play a role in the formation of blue wings in semi-regular variables and rarely in Miras. However, we did not observe that all semi-regulars and Miras showed blue wing emission without red counterpart whichever optical phase we observed. This tends to prove that turbulence does not dominate, but may nevertheless contribute to the formation of the line wings.

#### 4.1.2. Stellar Pulsation

The fact that our data show for most stars in our sample a rather regular pattern for the variations of  $R_{21}$  with the optical phase demonstrates that some connection exists between the stellar pulsation and the occurrence of SiO line wings. Therefore, the stellar pulsation induces variations of the ratio  $R_{21}$  with a maximum activity consistent with the 0.1-0.3 phase lag observed in the bulk of the SiO emission with respect to the stellar flux. (In fact, the SiO maser main intensity follows the IR luminosity with optical phase lags 0.1 – 0.3 and 0.6 – 0.8 for maxima and minima, respectively.) Several observations in R Leo confirm this result. But the stellar pulsation can induce variations in the line wing emission in two different ways: directly by shocks, or indirectly by luminosity variations. Concerning the shocks, several models have attempted to predict the behaviour of the outer atmospheric gas layers in pulsating late-type variables (e.g. Bowen 1988, Wood 1989). The non-linear pulsation model of Wood (1989) successfully explains the velocity changes observed for the hydrogen lines in Miras. The shock wave generated at each pulsation cycle is responsible for the velocity discontinuity. This is also in agreement with the IR line observations of Hinkle et al.(1984) showing both photospheric material and outwardly moving gas (post-shock material), and with the results of Boboltz et al.(1997) who observed SiO masers undergoing infall in R Aqr. In these conditions the radial velocities may exceed the terminal velocity of the associated circumstellar envelope as this is the case for our SiO observations. Similar predictions are made by Bowen's (1988) model where the stellar pulsation generates outflowing and infalling gas layers which could be responsible for our blue and red SiO wings. Velocities larger

than the terminal velocity are also predicted in the innermost layers of the envelope. In fact, the outflowing gas layer running into the infalling gas creates a shock wave which locally modifies the physical conditions, and in particular increases the local density of hydrogen, making maser emission more favourable at these higher velocities. (Note that this does not necessarily imply that collisions are dominant although the results of Miyoshi et al.(1994) suggest that collisional pumping plays a role for the bulk of the SiO emission.) On the other hand, if radiative pumping dominates, the observed variations of the line wing emission should correspond to maximum pumping efficiency around the optical phase 0.2 and minimum efficiency around phase 0.6. A change by a small factor in the fully saturated peak emission may imply an enormous factor for the unsaturated wings. In conclusion stellar flux variations and shock waves are important to explain our observations and maser emission, even if it is not easy to trace shocks by studying the SiO maser. Shocks may explain that there is SiO emission at high velocities, and radiative pumping may explain the variations of  $R_{21}$ .

The strong variations at a given phase from one cycle to another of  $R_{21}$ , of the main emission temperature  $T_{MB}$  and of the velocity observed in R And, TX Cam, RU Her and R Aql, as well as the changes in the SiO line wing emission observed in R Leo for different stellar cycles suggest that variations of the stellar physical conditions imply sudden changes in the SiO wing and main line emissions. These variations cannot be ascribed to changes in  $\Delta V(CO)$  which was found to remain constant at all epochs. Sudden changes are perhaps related to non-periodical stellar structure changes implying changes in the SiO masing conditions. On the other hand, we cannot exclude the hypothesis of an overtone stellar pulsation mode which could induce short-time variations of the physical parameters, and thus of the SiO emission. Rapid changes of the main and wing line emissions could also be explained by sound waves which induce local variations in the density and relative velocity just above the stellar photosphere. We thus expect SiO line variations within short time scales. Pijpers et al.(1994) observed indeed in R Leo and R Cas variations of the intensity and velocity of the  $v = 1, J = 1 \rightarrow 0$  line over short periods of order 10-20 days. These sound waves could modify the SiO main and wing line emissions if both emissions were co-located.

#### 4.2. Location of the SiO line wings

Interferometric observations of the SiO line wings would of course be indispensable to accurately locate the red and blue line wing emissions within the circumstellar envelope. There is at least one known case, that of R Leo, for which blue and red SiO wings are not coexistent. This was demonstrated by the lunar occultations made by Cernicharo et al.(1994) and by the relative position measurements made with the IRAM interferometer (Baudry et

al.1995). We note that, in the absence of interferometric data, the observation of phase lags between the SiO wing and bulk emissions could in principle indicate different spatial locations. However, in the case of variations in the radiative pumping resulting from stellar flux variations one would expect very small and thus not observable phase lags, whereas in the case of dominant shock fronts the propagation is slower, and may induce only very long-term phase lags. On the other hand, and despite our lack of more densely sampled observations, our study of the ratio  $R_{21}$  with the stellar light cycle gives indirect evidence for similar conditions of excitation for the SiO wings and the bulk of the SiO emission. We have found that the maximum value of the ratio  $R_{21}$ , namely the maximum activity in the line wings, tends to occur when the maximum activity also occurs in the bulk of the SiO emission. This seems to be the general trend for most stars in our sample (see Sect. 3.3). In addition, for those stars in which we have observed sudden variations of the amplitude of  $R_{21}$  we have observed simultaneous variations of  $T_{MB}$  and velocity. This suggests again that the main SiO line emission and the SiO line wings require similar pumping mechanisms, although they might not be excited in the same gas layers with similar physical conditions (e.g. different SiO column densities).

In order to deepen the physical meaning of the ratio  $R$ , we have plotted the values of  $R$  obtained at the four epochs of our observations versus the stellar mass loss rate  $dM/dt$  taken from Loup et al. (1993). For both  $R_{21}$  and  $R_{32}$ ,  $R$  decreases with increasing mass loss rate, with two notable features for  $R_{21}$  (Fig. 7): a sudden increase for mass loss rates around  $5 - 9 \cdot 10^{-7} M_{\odot}/\text{yr}$ , and a broad plateau where  $R_{21}$  stays low and roughly constant for  $dM/dt$  between  $10^{-6}$  and  $10^{-5} M_{\odot}/\text{yr}$ . We note, however, that the main features in Fig. 7 would deserve confirmation with additional data, and that the scatter present in the plot  $R_{21} = f(dM/dt)$  may also be due to uncertainties in the mass loss rates. In fact, our sample is biased because of a dependence of  $dM/dt$  on the distance in the range 100 pc to 400 pc (sensitivity limitation). Nevertheless, even for the most distant stars, the detection rate of line wing emission is comparable to that for the closest stars. Because  $\Delta V(\text{CO})$  is a good indicator of the expansion of the envelope while  $\Delta V(\text{SiO})$  is closely related to both the excitation and the kinematics of SiO we have plotted separately  $\Delta V(\text{CO})$  and  $\Delta V(\text{SiO})$  versus  $dM/dt$  for our sample stars. As expected for a species excited far in the envelope,  $\Delta V(\text{CO})$  increases with  $dM/dt$ ; we also observe a flattening for the highest mass loss rates. On the other hand,  $\Delta V(\text{SiO})$  does not clearly exhibit the general decrease observed in the plot  $R_{21} = f(dM/dt)$ . Therefore, this decrease as well as the flattening observed for  $R_{21}$  seem to be readily explained by the general behaviour of  $\Delta V(\text{CO})$  in our sample. These plots demonstrate that the regions of SiO wing emission and CO expansion are not directly related and strongly support the idea that the

SiO wing emission arises from the innermost circumstellar layers (although we cannot say it coexists entirely with the bulk of the SiO emission). The apparent peak of SiO wing emission observed in Fig. 7 suggests that, to excite this emission, more favourable pumping conditions (e.g. adequate densities) may exist around  $5 - 9 \cdot 10^{-7} M_{\odot}/\text{yr}$ . However, we are unable at the moment to specify error bars on the mass-loss rates, and therefore the reality of the peak for the ratio  $R_{21}$  must be confirmed by newer observations obtained for a larger sample of stars.

## 5. Conclusions

We have observed a rather large sample of late-type stars including Miras and semi-regulars with the IRAM 30-m radiotelescope at four epochs covering the period 1994 to 1996 in order to investigate the correlation between the SiO line wing activity and the stellar light phase. The SiO  $v = 1, J = 2 \rightarrow 1$  and  $J = 3 \rightarrow 2$  lines were observed simultaneously with the CO  $J = 2 \rightarrow 1$  quasi-thermal emission line. Several high velocity wings have been detected in the red and blue edges of the SiO profile.

The SiO wing emission could result from complex mechanisms combining stellar pulsation of the fundamental mode, and perhaps of other modes, with asymmetric mass loss (as for R Leo) and structure changes. We deduce from our observations that the time evolution of the SiO line wings is related to the stellar pulsation. However, it is difficult to specify how the pulsation induces local physical variations responsible for variations of the SiO wing emission. Pulsation, through shocks, may produce high velocity emissions which then vary according to the optical phase. For the semi-regular variables there is some indication on the importance of turbulent motions in the formation of the high velocity emission as well.

Finally, we have shown that the SiO wing emission results from masing processes and that this emission very likely arises from the innermost gas layers of the circumstellar envelope.

*Acknowledgements.* We thank the IRAM personnel at the 30-m telescope for their efficient help during the observations and we thank P.J. Diamond and E. González-Alfonso for very useful comments. Part of this work was supported by the CNRS URA 352. This research has made use of the AFOEV database, operated at CDS, France.

## References

- Alcolea J. 1993, Ph.D. Thesis, Madrid
- Baudry A., Lucas R., Guilloteau S. 1995, A&A 293, 594
- Boboltz D.A., Diamond P.J., Kemball A.J. 1997, ApJ 487, L147
- Bowen G.H. 1988, ApJ 329, 299
- Bujarrabal V., Gomez-Gonzalez J., Planesas P. 1989, A&A 219, 256
- Bujarrabal V., Alcolea J., Sanchez-Contreras C., Colomer F. 1996, A&A 314, 883

- Cernicharo J., Brunswig W., Paubert G., Liechti S. 1994, ApJ 423, L143
- Cernicharo J., Alcolea J., Baudry A., González-Alfonso E. 1997, A&A 319, 607 (CABG)
- González-Alfonso E. & Cernicharo J. 1997, A&A 322, 938
- Herpin F. 1998, Ph.D. Thesis, Université de Bordeaux
- Hinkle K.H., Scharlach W.W.G., Hall D.N.B. 1984, ApJS 56, 1
- Huggins P.J. & Healy A.P. 1986, ApJ 304, 418
- Loup C., Forveille T., Omont A., Paul J.F. 1993, A&ASS 99, 291
- Martinez A., Bujarrabal V., Alcolea J. 1988, A&ASS 74, 273
- Miyoshi M., Matsumoto K., Kamenno S., Takaba H., Iwata T. 1994, Nat. 371, 395
- Pijpers F.P., Pardo J.R., Bujarrabal V. 1994, A&A 286, 501
- Wood P.R. 1989, "From Miras to Planetary Nebulae", Editions Frontières, edited by M.O.Menessier and A.Omont